

LES of Turbulent Flows: Lecture 22

(ME EN 7960-008)

Prof. Rob Stoll
Department of Mechanical Engineering
University of Utah

Spring 2011

Evaluating Simulations and SGS models

- How do we go about testing our models? How should models be validated and compared to each other?
- Pope (2004) gives 5 criteria for evaluating SGS models:
 1. Level of description in the SGS model
 2. Completeness of the model
 3. The cost and ease of use of the model
 4. The range and applicability of the model
 5. The accuracy of the model
- Most of these criteria are related to the accuracy of simulation results:
 - Accuracy**: Ability of the model to reproduce DNS, experimental or theoretical statistical features of a given test flow (or the ability to converge to these values with increasing resolution)

An important aspect of this is **grid convergence of simulation statistics**. This is not always done but is an important aspect of simulation validation. Note that this convergence (especially in high-Re flows) may not be exact, we may only see approximate convergence.

Evaluating Simulations and SGS models

-**Cost**: When examining the above, it is important to include the cost of each model (and comparisons between alternative models).

-One model may give better results at a lower grid resolution (larger Δ) but include costs that are excessive:

Example: Scale-dependent Lagrangian dynamic model (Stoll and Porté-Agel, WRR, 2006):

38% increase in cost over constant Smagorinsky model

15% increase over plane averaged scale-dependent model

How much of a resolution increase can we get in each direction for a 30% cost increase?? Only a little more than 3% in each direction!

-**Completeness**: A “complete” LES and SGS model would be one that can handle different flows with simply different specification of BCs, initial conditions and forcings.

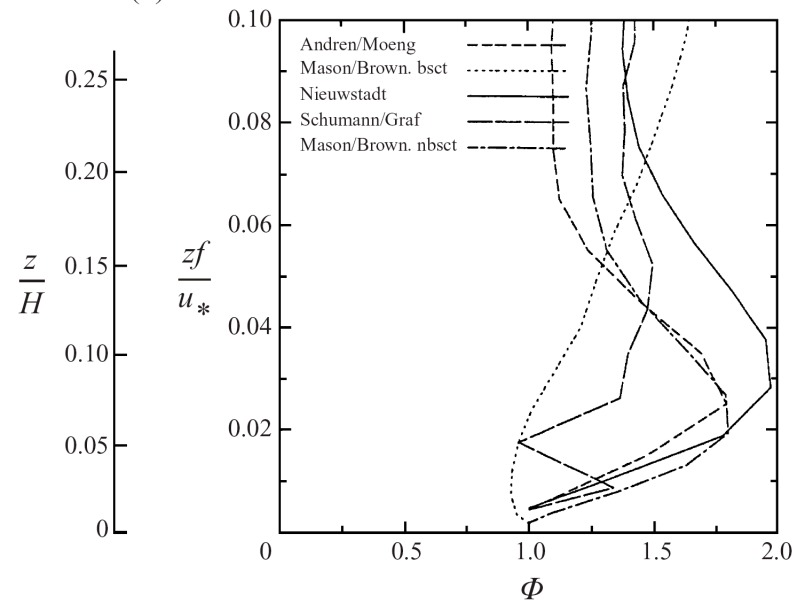
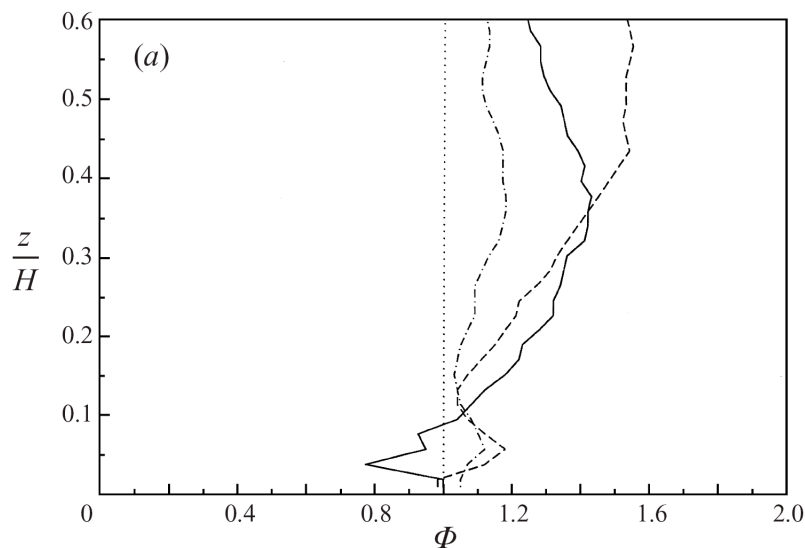
-In general LES models are not complete due to grid requirements and (possibly) ad hoc tuning for different flows.

-Example from RANS: mixing length models are incomplete (different flow different l) while the k - ϵ model can be thought of as complete for RANS since it can be applied to any flow.

Accuracy of LES models

- Here we will look at some examples of different measurements of simulation accuracy and evaluation as well as a few common test cases for LES

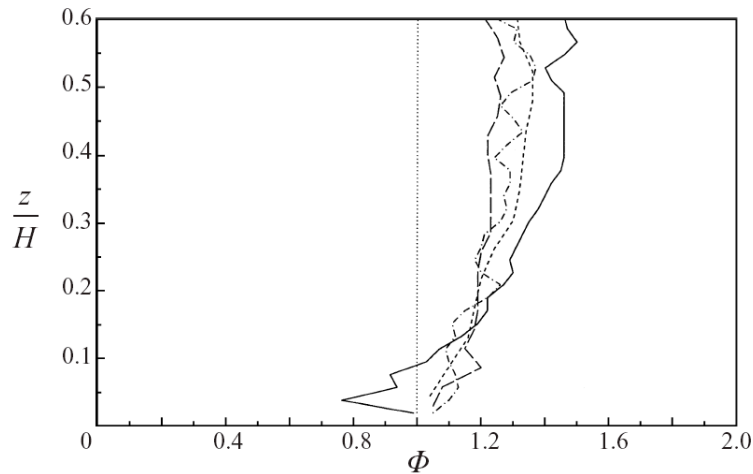
- An example of the accuracy of LES models to predict flow statistics (from Porte-Agel et al, JFM 2000 and Andren et al., 1994, QJRMS):



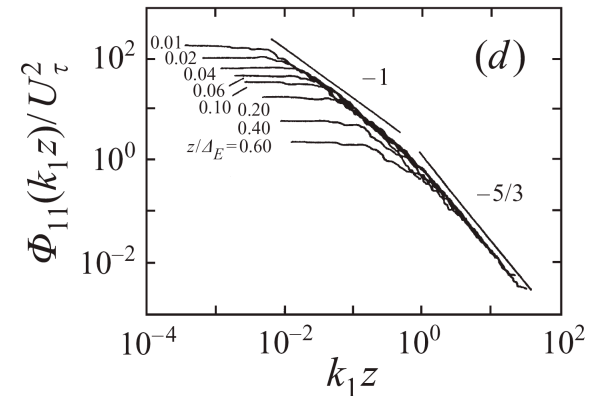
- Non-dimensional velocity gradient

Accuracy of LES models

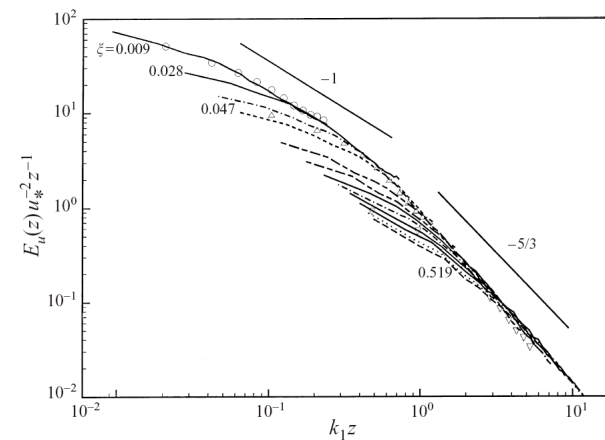
- An example of the accuracy of LES models to predict flow statistics (from Porte-Agel et al, JFM 2000)



- Non-dimensional velocity gradient



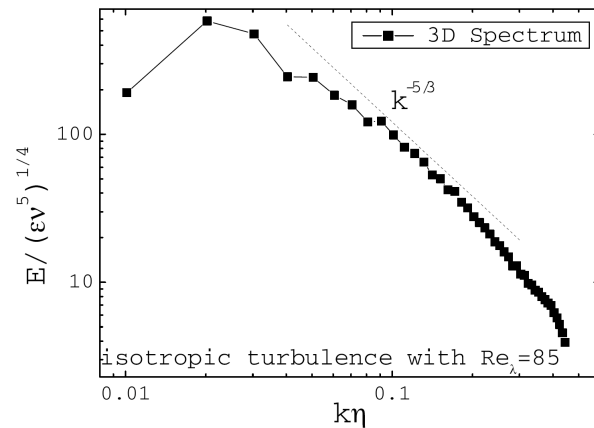
- Streamwise velocity spectra from Perry et al (1986)



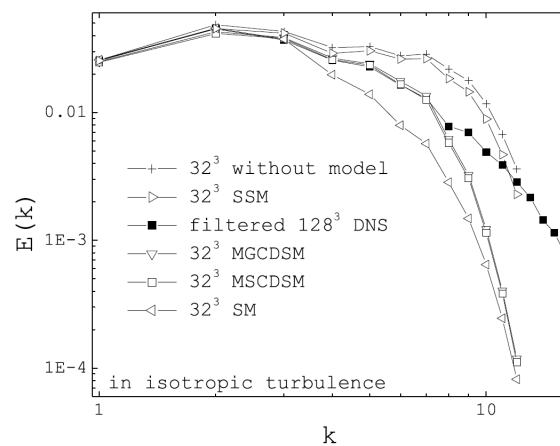
- Streamwise velocity spectra at two different resolutions

Test Case: Isotropic Turbulence LES

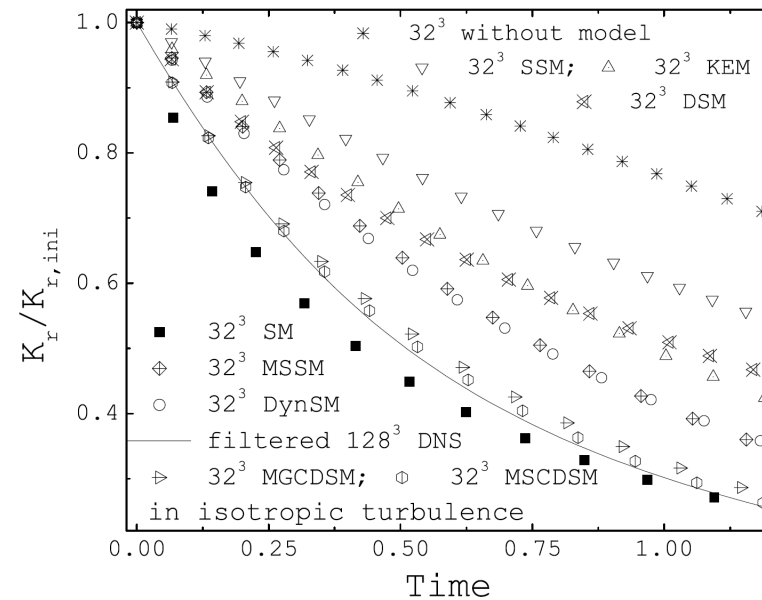
- An example from Lu et al, 2008



- Velocity spectra from DNS



- Velocity spectra from filtered DNS and LES



- Energy decay in isotropic turbulence

Test Case: Turbulent Boundary Layers

- An example from Guerts, 2004 of the effect of different SGS models on boundary layer development

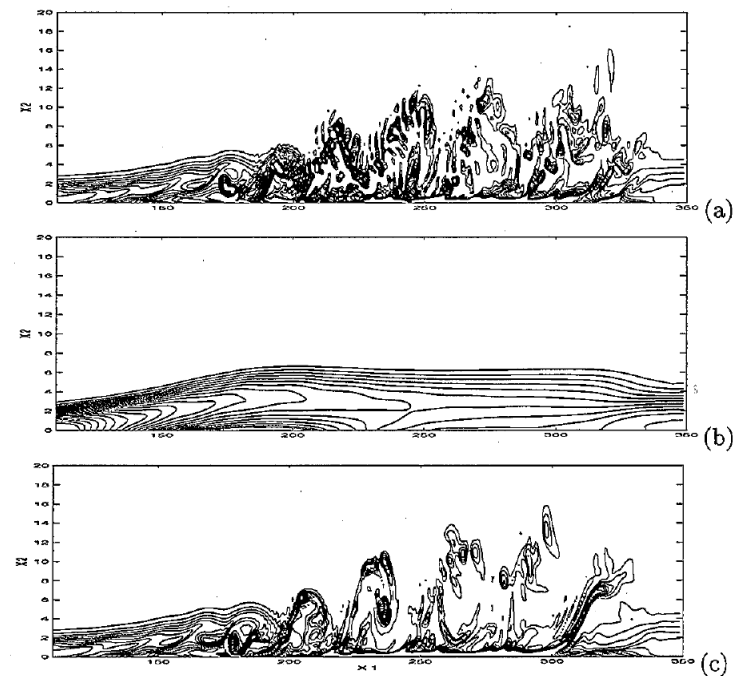


Fig. 8.15. Snapshot of the spanwise vorticity component: (a) DNS prediction, (b) LES with Smagorinsky's model and van Driest damping, (c) LES with dynamic eddy-viscosity model.

Test Case: Backward Facing Step

- An example from Cabot and Moin, 2000

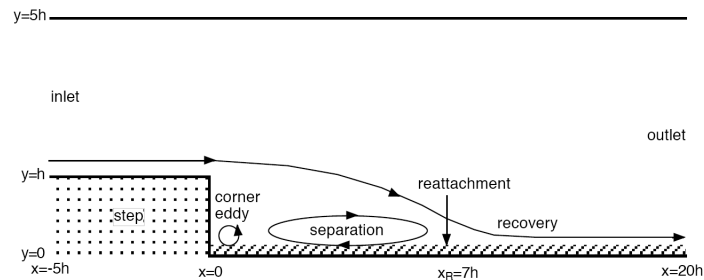


Figure 4. Sketch of the simulation domain for flow over a step of height h with an expansion ratio of 4 to 5. Wall stress models were used in the hatched region.

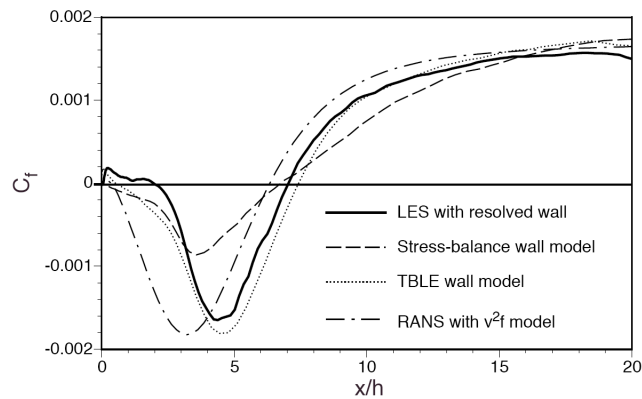


Figure 6. Friction coefficient on the bottom wall behind a step for the wall-resolved LES [2], wall stress models using stress balance and TBLE with a dynamic kappa in equation (5), and a global RANS v^2f model [18].

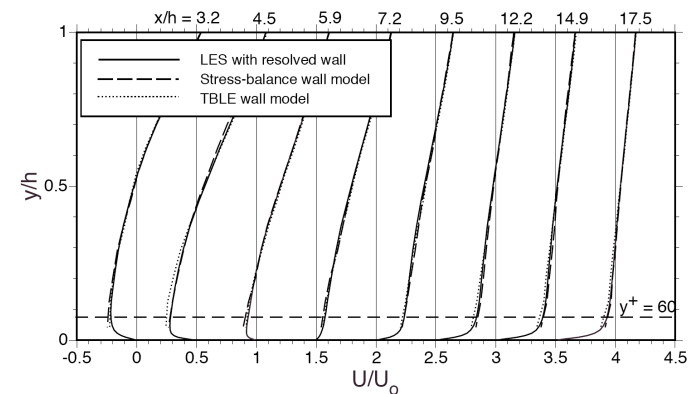


Figure 7. Mean streamwise velocity at different stations behind a step for the wall-resolved LES [2], and stress-balance and TBLE wall stress models. The dashed line is the height of the first computational cell, about 60 wall units near the exit.

Boundary Conditions for LES

Boundary Conditions:

- Like all numerical techniques for PDEs, LES requires the specification of boundary conditions:
 - Lateral or inflow/outflow conditions
 - Boundary conditions at solid walls (particularly interesting for LES)
 - Note in some flows top (upper) boundary conditions are also important. The most common example (I know of) is of the ABL when buoyancy effects are present resulting in gravity waves. The two most common ways of dealing with this:
 - Rayleigh dampening where a sponge layer of points is defined
 - Linear wave canceling (Klemp and Durran, MWR, 1983)
 - Initial conditions (for time integration) can also be an important issue for some flows (e.g., decaying isotropic turbulence)
- Here we will talk about inflow boundary conditions and boundary conditions at solid boundaries

Need for Proper Inflow Conditions

Inflow Boundary Conditions:

- Issues related to lateral (flow direction) BCs are not specific to LES. In DNS nearly identical issues are present. In RANS (many times) this issue is not important since appropriate conditions based on mean fields are all that is needed.

- **Simplest case: Periodic BCs**

What goes out comes back in (identically).

- For true BL flow (that grow in the flow direction) or flows with complex geometry, **many times we can't use periodic BCs.**

- The figure and caption to the right illustrate **the importance of proper inflow BCs in a turbulent flow.**

- Here we will cover a few ways to deal with this (see Sagaut Ch 10.3)

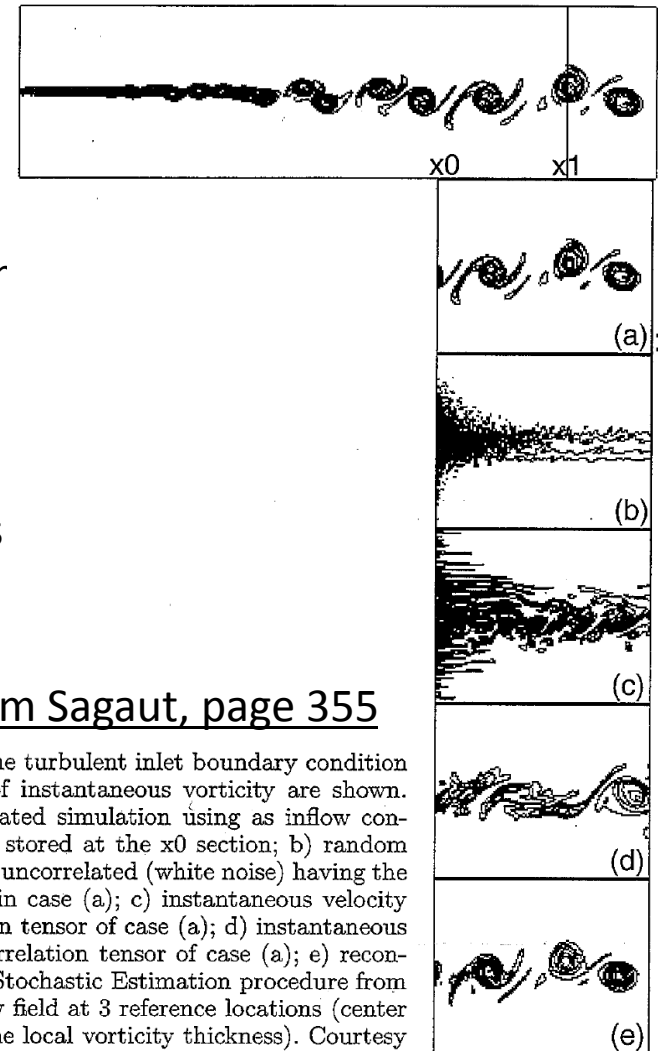


Figure and caption from Sagaut, page 355

Fig. 10.16. Illustration of the influence of the turbulent inlet boundary condition (DNS of a 2D mixing layer). Iso-contours of instantaneous vorticity are shown. *Top:* reference 2D simulation. *Below:* Truncated simulation using as inflow conditions: a) exact instantaneous velocity field stored at the x_0 section; b) random velocity fluctuations spatially and temporally uncorrelated (white noise) having the same Reynolds stress tensor components as in case (a); c) instantaneous velocity field preserving temporal two point correlation tensor of case (a); d) instantaneous velocity field preserving spatial two point correlation tensor of case (a); e) reconstructed velocity field with the aid of Linear Stochastic Estimation procedure from the knowledge of exact instantaneous velocity field at 3 reference locations (center of the mixing layer and $\pm\delta_\omega/2$ where δ_ω is the local vorticity thickness). Courtesy of Ph. Druault and J.P. Bonnet, LEA.

Precursor Simulations Inflow Conditions

Precursor Simulations:

- One of the most effective ways to generate inflow conditions is to specify inflow from “homogeneous” (for example horizontally) pre-run flow simulations.

Figure from
Sagaut, page 362

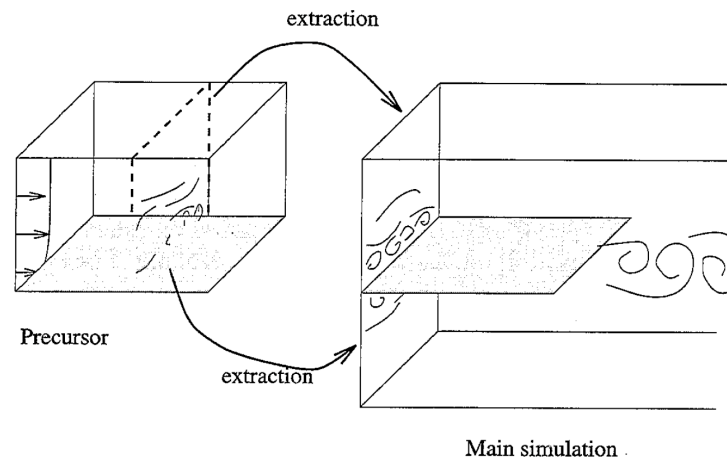


Fig. 10.17. Schematic of the precursor simulation technique. A precursor simulation of an attached boundary layer flow is performed. An extraction plane is defined, whose data are used as an inlet boundary condition for a simulation of the flow past a trailing edge.

- **Pros:** requires very few assumptions and we don't need an “adjustment” zone (as many other techniques do)
- **Cons:** Precursor simulations can be expensive (sometimes as much as the actual simulation of interest!).

Rescaling

- Almost all other techniques try to specify: $\tilde{u}(x_o, t) = \langle \tilde{u}(x_o) \rangle + u'(x_o, t)$
- Many of these techniques **use an assumed energy spectrum** combined with assumed BL profiles (see Sagaut pg 356 for a list) or require other *a priori* knowledge of turbulence statistics of the exact flow.
- Another method is to **rescale the flow**.
 - with this technique (shown in the figure to the right), the flow from a downstream location, separated from the inflow enough to be considered independent is scaled (using know flow properties) to become the new inflow.
 - The technique was developed by Lund et al., J. Comp. Phys 1998.

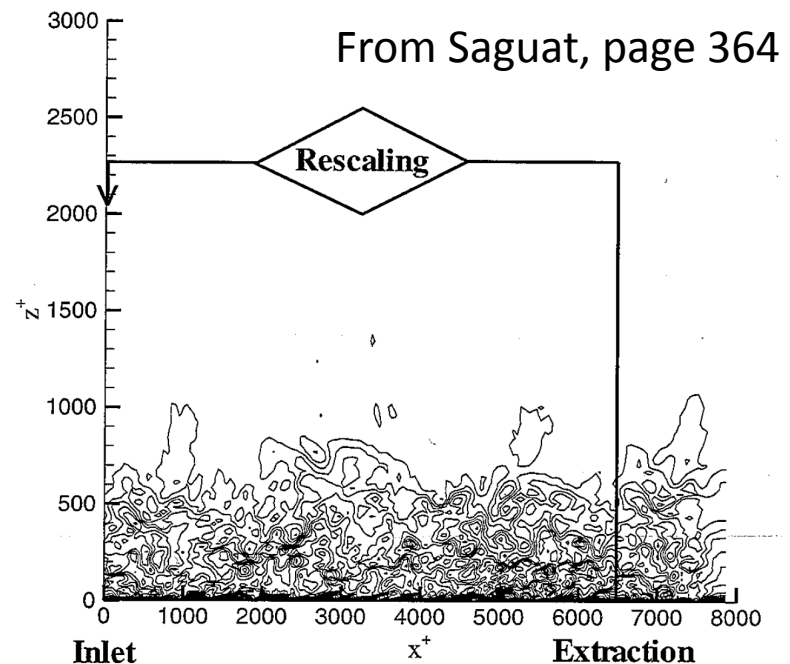



Fig. 10.18. Schematic of Lund's extraction/rescaling technique. Instantaneous isolevels of streamwise velocity in a boundary layer are shown. Courtesy of E. Tromeur and E. Garnier, ONERA.

Surface/wall Boundary Conditions

- In many flows of interest a solid wall (or surface) is present in some way.
 - It can be very costly to fully resolve the effects of the wall and implement “natural” no-slip BCs
 - Chapman (1979, AIAA) performed the first analysis of grid-resolution requirements for LES of wall-bounded flows.
 - We can divide the flow into 2 regions:
 - outer layer:** viscosity isn’t as important and grid resolution requirements are more or less (not including SGS model errors) independent of Re
 - inner layer:** near wall region where viscosity plays an important role.
 - Structures (“eddies”) in the inner-layer are approximately constant when non-dimensionalized with viscous length scales.
 - To resolve these motions we need grid spacing of:
 - $\Delta x^+ \sim 100$ ($x^+ = x_i u_\tau / \nu$)
 - $\Delta z^+ \sim 20$
-  friction velocity

Requirements to Resolve the Wall

- Using these Δx^+ and Δz^+ scales we can show that: $N_x \times N_y \times N_z \propto Re_L^{1.8}$ if we want to resolve the viscous sublayer (to enforce use the no slip condition). └─┬─> integral Re
- For a BL with $Re_L = 10^6$ (moderate-low Re) **99% of our points** will need to be in the near wall region whose thickness is **only 10% of the entire boundary layer!**

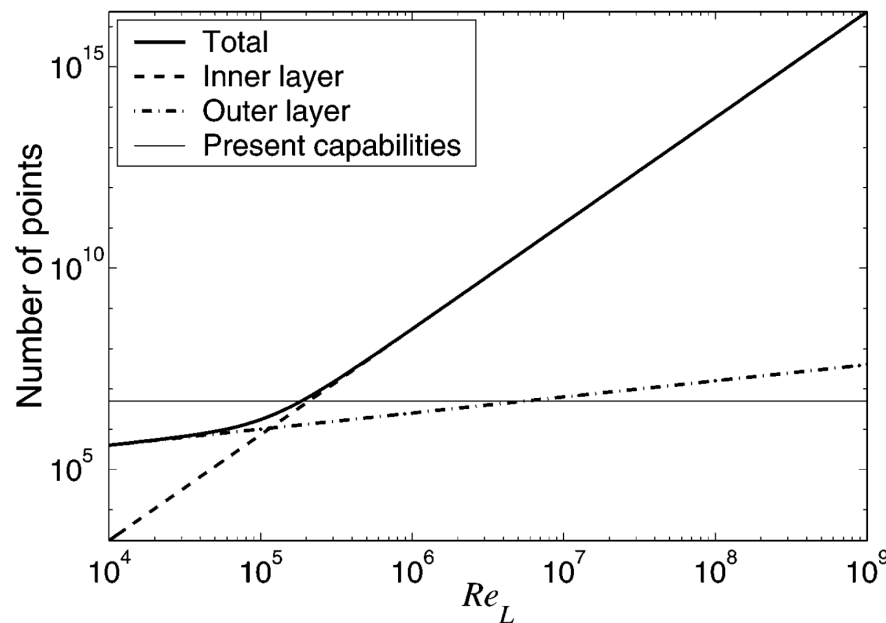


Figure from Piomelli and Balaras, ARFM, 2002

Figure 1 Number of grid points required to resolve a boundary layer. The “Present capabilities” line represents calculations performed on a Pentium III 933MHz workstation with 1Gbyte of memory.

Approximate wall-boundary conditions

- How do we handle this problem for high-Re boundary layers?

- Answer: with **approximate wall-boundary conditions**:

- We **pick our first grid-point** to be sufficiently far from the wall so it lies **in the outer layer**.

- This has the **potential** to make our **simulations only weakly dependent** on Re and grid resolution (if we don't consider model errors!)

- The **goal is to create a model** that calculates the **wall shear stress as a function of the resolved velocity** at the lowest grid level.

- All of the dynamics of the inner layer** must be accounted for with the wall model.

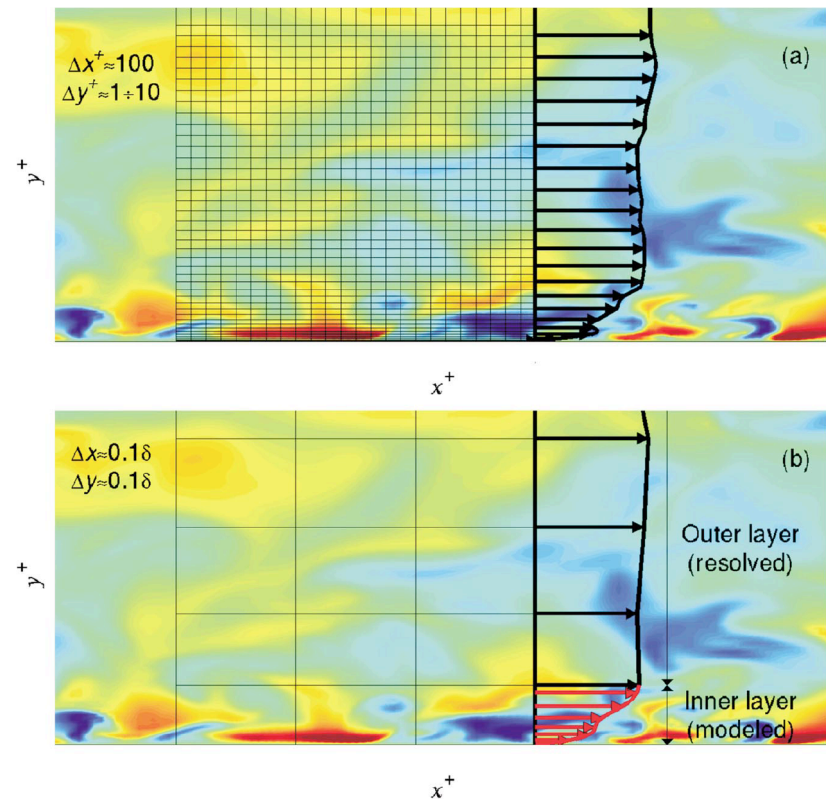


Figure 2 Sketch illustrating the wall-layer modeling philosophy. (a) Inner layer resolved. (b) Inner layer modeled.

From: Piomelli and Balaras, ARFM, 2002

Approximate wall-boundary conditions

• Typical high-Re wall models:

-Many wall models use RANS-like approximations

-In high-Re BLs, the most common models are 0th order RANS (i.e. similarity theory).

- \tilde{u}_i and τ_w are assumed to be related by the well known log-law:

for a rough-wall =>
$$U(z) = \frac{u_\tau}{\kappa} \left[\ln \left(\frac{z}{z_o} \right) - \Psi_M \left(\frac{z}{L} \right) \right]$$

mean velocity
= $\sqrt{-\tau_w}$
roughness
stability correction

→ height of 1st grid point

-Schumann (1975) introduced the 1st of this class of models where:

$$\tau_{i3,w}(x, y, t) = \langle \tau_w \rangle \frac{\tilde{u}_i(x, y, z, t)}{U(z)} \quad \text{for } i=1,2 \text{ (x,y)}$$

and where $\langle \tau_w \rangle$ was calculated from the mean pressure gradient.

-Grötzbach (1987) modified this by using the log-law to calculate the average shear stress resulting in the flowing model

$$\tau_{i3,w}(x, y, t) = - \left[\frac{U(z)\kappa}{\ln(z/z_o) - \Psi_M} \right] \left[\frac{\tilde{u}_i(x, y, z, t)\kappa}{\ln(z/z_o) - \Psi_M} \right]$$

This model has the advantage over Schumann's by allowing the total mass flux to change in time during a simulation. Both models assume that $\tau_w \sim \tilde{u}_i$

Accounting for flow average flow structures

- Piomelli et al., (PoF, 1989) altered the models of Schumann and Grötzbach in an attempt to account for the structure of the flow field.
- Experimental and numerical studies have demonstrated that **coherent structures** exist in the BL and that they are **inclined at oblique angles to the wall** (e.g. Brown and Thomas, PoF 1977).
- The inclination of these structures can be measured by looking at the correlation between shear stress and velocity in a BL. With the average inclination given by the **lag to max correlation with height**.
- Piomelli et al. (1989) took this into account by Shifting the SG model downstream:

$$\tau_{i3,w}(x, y, t) = \langle \tau_w \rangle \frac{\tilde{u}_i(x + \delta_d, y, z, t)}{U(z)}$$

Where the displacement $\delta_d = z \cot \gamma$

And $\gamma \approx 13^\circ$ for high Re flows.

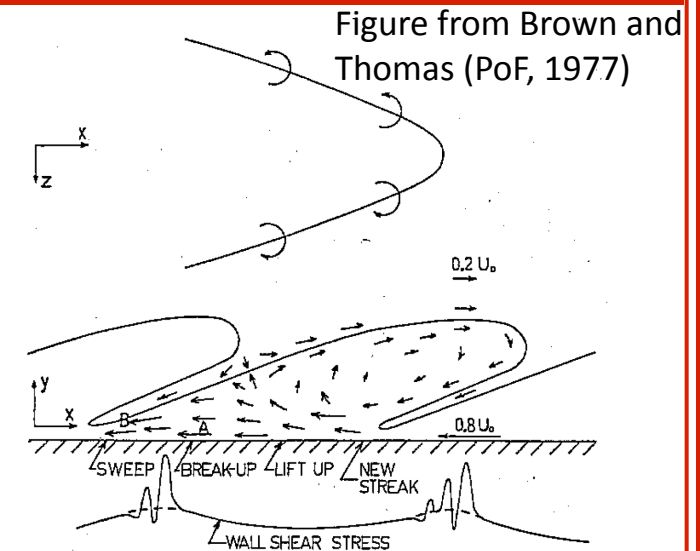


FIG. 12. Proposed flow pattern that might be seen by an observer moving at a speed of $0.8 U_0$, and the associated wall shear stress distribution.

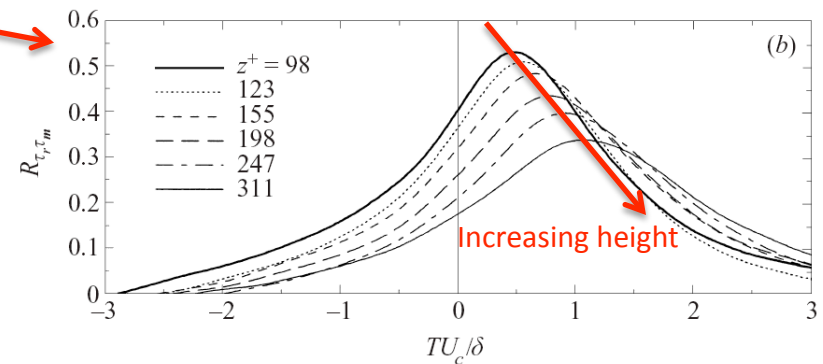


Figure from Masusic et al. (JFM, 2001)

Local and Higher-order RANS approximations

- **The local log-law for ABL flows:**

-In the ABL or general flows where no directions of homogeneity exist for determining $\langle \tau_w \rangle$ the log-law is many times used directly to calculate the local shear stress by:

$$\tau_{i3,w}(x, y, t) = - \left[\frac{\tilde{u}_r(x, y, z, t) \kappa}{\ln(z/z_o) - \Psi_M} \right]^2 \left[\frac{\tilde{u}_i(x, y, z, t)}{\tilde{u}_r(x, y, z, t)} \right]$$

where $\tilde{u}_r = \sqrt{\tilde{u}_x^2 + \tilde{u}_y^2}$

-This formulation assumes $\tau_w \sim \tilde{u}_i^2$ and does not preserve $\langle \tau_w \rangle$.

- **2-layer models (higher-order RANS):**

Balaras et al., (AIAA, 1996) used a higher order RANS closure based on the thin-BL equations:

$$\frac{\partial \tilde{u}_i}{\partial t} + \frac{\partial}{\partial x_i} (\tilde{u}_n \tilde{u}_i) = - \frac{\partial \tilde{p}}{\partial x_i} + \frac{\partial}{\partial x_n} \left[(\nu + \nu_t) \frac{\partial \tilde{u}_i}{\partial x_n} \right]$$

where $i=1,2$, u_n is the wall normal component found from continuity and ν_t is an eddy-viscosity parameterized with an algebraic model. The equations are solved to the wall.

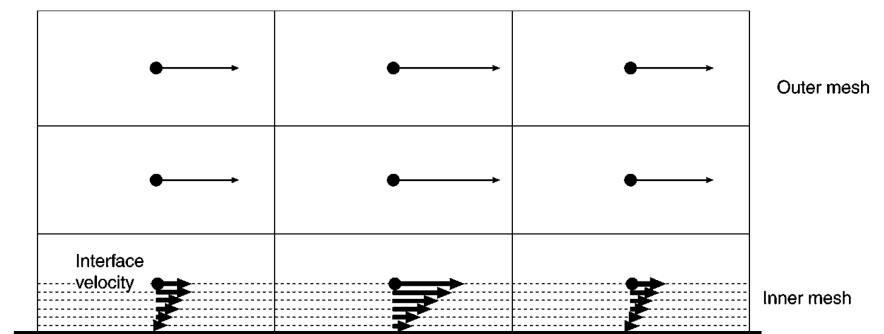


Figure 4 Inner-and outer-layer grids for the two-layer model.

Figure from Piomelli and Balaras, 2002

Comparing different models a posteriori

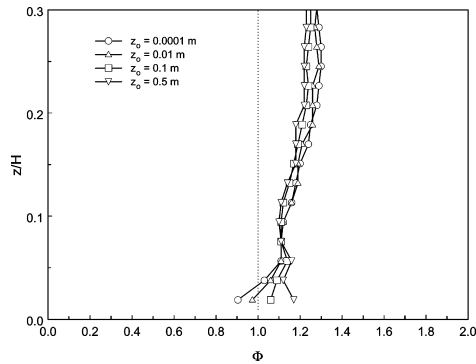


Figure 2. Non-dimensional gradient of the mean streamwise velocity $\Phi = \frac{\sum_{i=1}^n \frac{du_i}{dz_i}}{u_*}$ from simulations that use the SG surface model over surfaces with four different aerodynamic roughness lengths z_0 . The height z is normalized with the boundary-layer depth H . The dotted line corresponds to the classical log-law (expected to hold on the lower 10% of the domain) with $\kappa=0.4$.

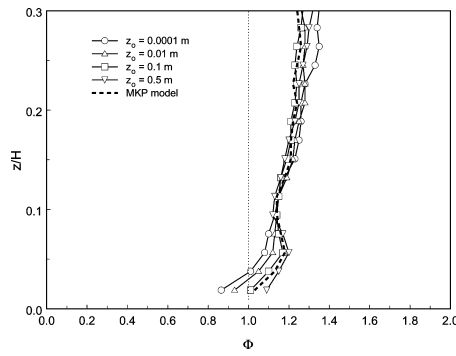


Figure 3. Non-dimensional gradient of the mean streamwise velocity $\Phi = \frac{\sum_{i=1}^n \frac{du_i}{dz_i}}{u_*}$ from simulations that use the shifted SG surface model over surfaces with four different aerodynamic roughness lengths z_0 . The height z is normalized with the boundary-layer depth H . The dashed line corresponds to the MKP model and a surface roughness $z_0=0.1$ m. The dotted line corresponds to the classical log-law (expected to hold on the lower 10% of the domain) with $\kappa=0.4$.

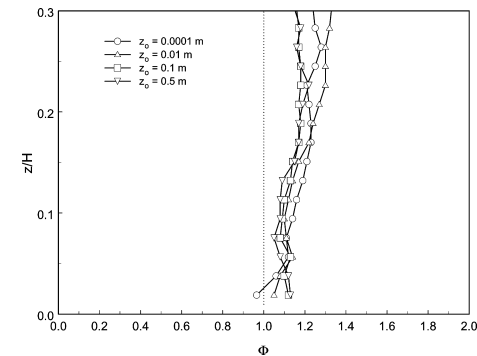


Figure 4. Non-dimensional gradient of the mean streamwise velocity $\Phi = \frac{\sum_{i=1}^n \frac{du_i}{dz_i}}{u_*}$ from simulations that use the local SG surface model over surfaces with four different aerodynamic roughness lengths z_0 . The height z is normalized with the boundary-layer depth H . The dotted line corresponds to the classical log-law (expected to hold on the lower 10% of the domain) with $\kappa=0.4$.

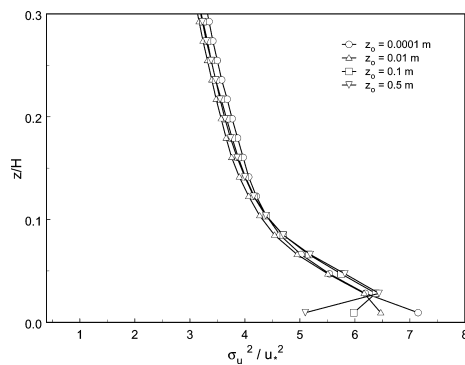


Figure 5. Vertical distribution of the normalized variance of the resolved streamwise velocity from simulations using the SG surface model over surfaces with four different aerodynamic roughness lengths z_0 . The height z is normalized with the boundary-layer depth H .

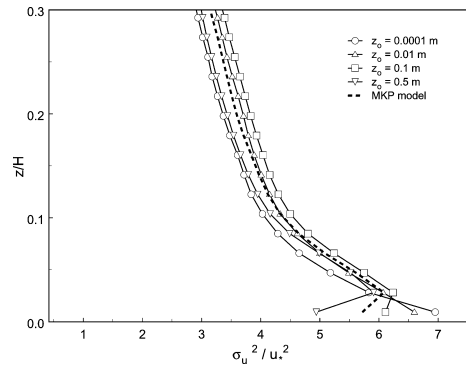


Figure 6. Vertical distribution of the normalized variance of the resolved streamwise velocity from simulations using the shifted SG surface model over surfaces with four different aerodynamic roughness lengths z_0 . The dashed line corresponds to the MKP model and a surface roughness $z_0=0.1$ m. The height z is normalized with the boundary-layer depth H .

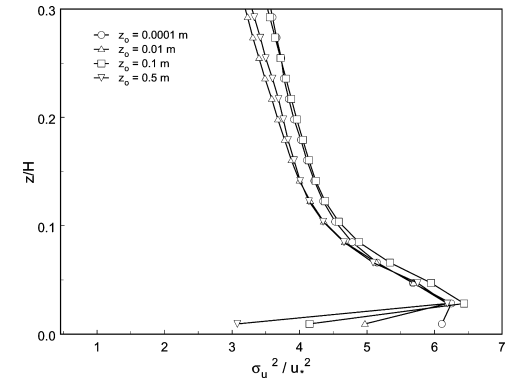


Figure 7. Vertical distribution of the normalized variance of the resolved streamwise velocity from simulations using the local SG surface model over surfaces with four different aerodynamic roughness lengths z_0 . The height z is normalized with the boundary-layer depth H .

Comparing different models a posteriori

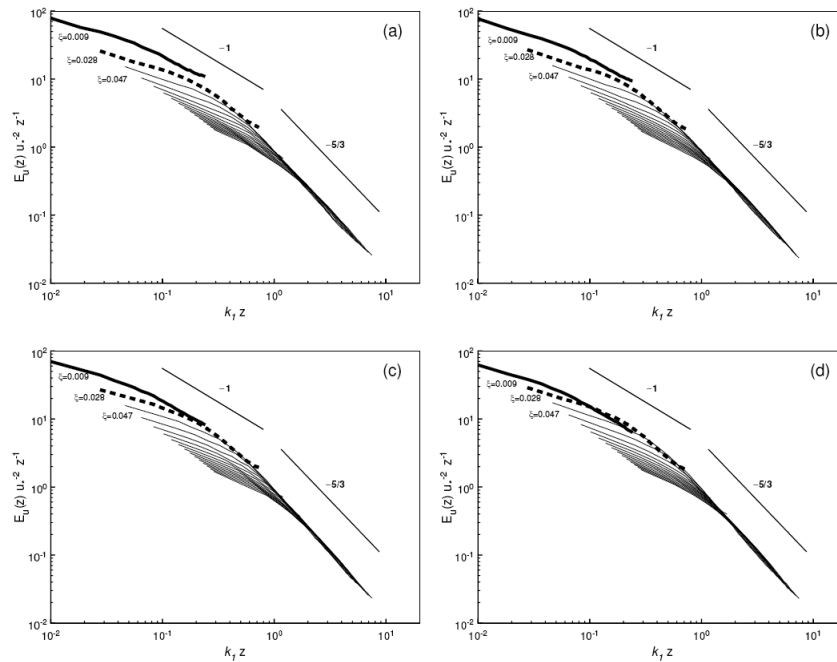


Figure 8. Normalized streamwise velocity spectra at different heights $\xi = z/H$ from simulations with the shifted SG model over surfaces with different aerodynamic surface roughness lengths: (a) $z_o = 0.0001$ m, (b) $z_o = 0.01$ m, (c) $z_o = 0.1$ m and (d) $z_o = 0.5$ m. The thick solid and dashed lines correspond to the first and second levels of computation at $\xi = 0.009$ and $\xi = 0.028$, respectively.

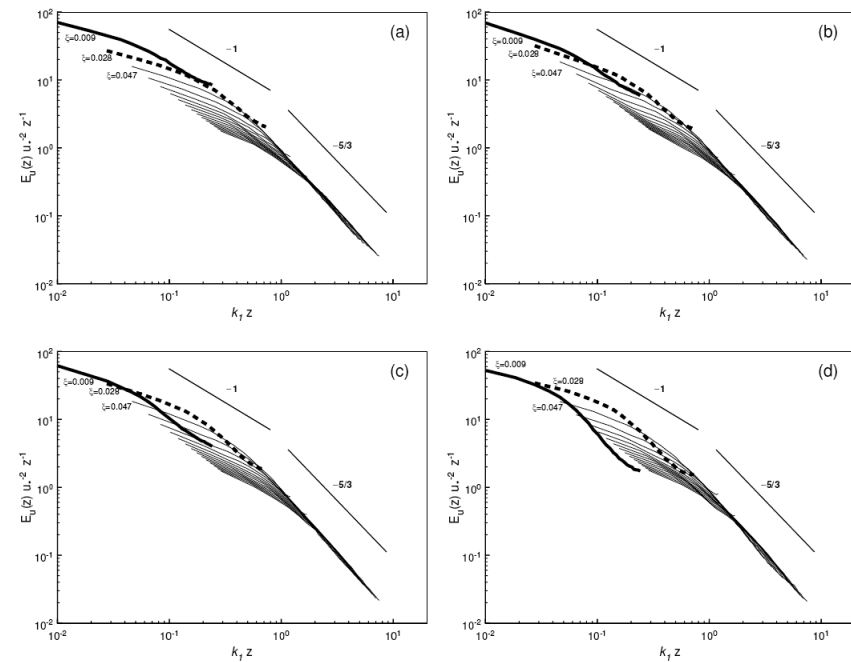


Figure 9. Normalized streamwise velocity spectra at different heights $\xi = z/H$ from simulations with the local SG model over surfaces with different aerodynamic surface roughness lengths: (a) $z_o = 0.0001$ m, (b) $z_o = 0.01$ m, (c) $z_o = 0.1$ m and (d) $z_o = 0.5$ m. The thick solid and dashed lines correspond to the first and second levels of computation at $\xi = 0.009$ and $\xi = 0.028$, respectively.